NASA/TP–2015–218569

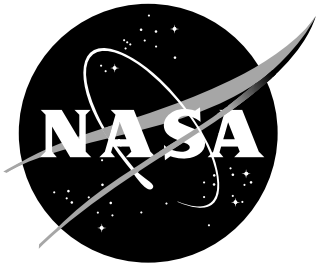

Badhwar - O'Neill 2014 Galactic Cosmic Ray Flux Model Description

P. M. O'Neill
NASA Johnson Space Center, Houston, Texas 77058, USA

S. Golge[†]
University of Houston, Houston, Texas 77004, USA

T. C. Slaba
NASA Langley Research Center, Hampton, Virginia 23681, USA

March 2015

[†]Also affiliated with: Space Radiation Analysis Group, NASA Johnson Space Center, Houston, Texas 77058, USA

NASA STI Program ... in Profile

Since its founding, NASA has been dedicated to the advancement of aeronautics and space science. The NASA scientific and technical information (STI) program plays a key part in helping NASA maintain this important role.

The NASA STI Program operates under the auspices of the Agency Chief Information Officer. It collects, organizes, provides for archiving, and disseminates NASA's STI. The NASA STI Program provides access to the NTRS Registered and its public interface, the NASA Technical Reports Server, thus providing one of the largest collections of aeronautical and space science STI in the world. Results are published in both non-NASA channels and by NASA in the NASA STI Report Series, which includes the following report types:

- TECHNICAL PUBLICATION. Reports of completed research or a major significant phase of research that present the results of NASA programs and include extensive data or theoretical analysis. Includes compilations of significant scientific and technical data and information deemed to be of continuing reference value. NASA counterpart of peer-reviewed formal professional papers, but having less stringent limitations on manuscript length and extent of graphic presentations.
- TECHNICAL MEMORANDUM. Scientific and technical findings that are preliminary or of specialized interest, e.g., quick release reports, working papers, and bibliographies that contain minimal annotation. Does not contain extensive analysis.
- CONTRACTOR REPORT. Scientific and technical findings by NASA-sponsored contractors and grantees.
- CONFERENCE PUBLICATION. Collected papers from scientific and technical conferences, symposia, seminars, or other meetings sponsored or co-sponsored by NASA.
- SPECIAL PUBLICATION. Scientific, technical, or historical information from NASA programs, projects, and missions, often concerned with subjects having substantial public interest.
- TECHNICAL TRANSLATION. English- language translations of foreign scientific and technical material pertinent to NASA's mission.

Specialized services also include organizing and publishing research results, distributing specialized research announcements and feeds, providing information desk and personal search support, and enabling data exchange services.

For more information about the NASA STI Program, see the following:

- Access the NASA STI program home page at ***http://www.sti.nasa.gov***
- E-mail your question to help@sti.nasa.gov
- Phone the NASA STI Help Desk at 757-864-9658
- Write to:
  NASA STI Information Desk
  Mail Stop 148
  NASA Langley Research Center
  Hampton, VA 23681–2199

NASA/TP–2015–218569

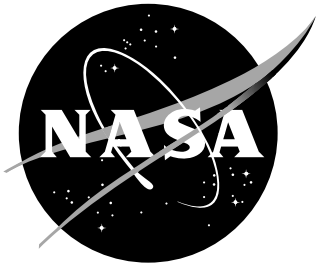

Badhwar - O'Neill 2014 Galactic Cosmic Ray Flux Model Description

P. M. O'Neill
NASA Johnson Space Center, Houston, Texas 77058, USA

S. Golge[†]
University of Houston, Houston, Texas 77004, USA

T. C. Slaba
NASA Langley Research Center, Hampton, Virginia 23681, USA

National Aeronautics and
Space Administration

Johnson Space Center
Houston, Texas 77058

March 2015

[†]Also affiliated with: Space Radiation Analysis Group, NASA Johnson Space Center, Houston, Texas 77058, USA

Acknowledgments

This work was partially funded by NASA under the Bioastronautics Contract (BC) number NAS902078. The authors would like to thank Dr. Mark Shavers for fruitful discussions on the model.

Abstract

The Badhwar-O'Neill (BON) Galactic Cosmic Ray (GCR) model is based on GCR measurements from particle detectors. The model has mainly been used by NASA to certify microelectronic systems and the analysis of radiation health risks to astronauts in space missions. The BON14 model numerically solves the Fokker-Planck differential equation to account for particle transport in the heliosphere due to diffusion, convection, and adiabatic deceleration under the assumption of a spherically symmetric heliosphere. The model also incorporates an empirical time delay function to account for the lag of the solar activity to reach the boundary of the heliosphere. This technical paper describes the most recent improvements in parameter fits to the BON model (BON14). Using a comprehensive measurement database, it is shown that BON14 is significantly improved over the previous version, BON11.

Contents

1 Introduction

It is well documented in the literature that the ionizing nature of Galactic Cosmic Ray (GCR) particles poses a potential health risk for crew members in space, particularly for future long-term missions in free-space [1–3]. Long-term exposure to the mixed (both low and high) Linear Energy Transfer (LET) GCR radiation significantly increases the Risk of Exposure Induced Cancer (REIC) and Risk of Exposure Induced Death (REID) [1–3]. As with exposure to any charged particle, GCR particles may interact with the cell at the deoxyribonucleic acid (DNA) level and cause DNA damage, and free-radical particle production.

Another major concern arises from the interaction of the GCR particles with the electronics inside and outside of a spacecraft. Energetic GCR particles may deposit energy in electronics, e.g., microprocessors, memory units, sufficient to cause memory bit flips and latch-up, which are called Single Event Effects (SEE) [4, 5].

In order to assess astronaut exposure and electronic effects associated with GCR exposure, models are used to describe relevant spectra of particles and energies appearing in deep space. These models formulate the GCR transport, associated energy loss mechanisms, which are also known as GCR modulation (either interstellar or in the solar system), and flux as a function of energy spectrum. The Badhwar-O'Neill (BON) model [6–9] numerically solves the Fokker-Planck (FP) equation that takes into account diffusion, convection, and adiabatic deceleration within the heliosphere. The solution to the FP equation as implemented in the BON model is the flux of GCR particles of a given charge, Z, as a function of energy. The solution is obtained under the assumptions of a quasi-steady state and a spherically symmetric interplanetary medium [10,11]. Under these assumptions, the FP equation can be written as [12]:

$$\frac{1}{r^2}\frac{\partial}{\partial r}(r^2 V_s U) - \frac{1}{3}[\frac{1}{r^2}\frac{\partial}{\partial r}(r^2 V_s)][\frac{\partial}{\partial T}(\alpha T U)] \quad = \quad \frac{1}{r^2}\frac{\partial}{\partial r}(r^2 \kappa \frac{\partial U}{\partial r}) \quad (1)$$

where r is the radial position in astronomical units (AU); T is the kinetic energy (MeV/n); $U(r,T)$ is the GCR flux (particles/sr·m^2·s·MeV/n), $V_s(r)$ the solar wind speed ($\approx$ 400 km/s); $\kappa(r,T)$ the particle diffusion coefficient tensor; and $\alpha(T) = (T + 2T_0)/(T + T_0)$, with T_0 being the rest energy of the GCR particle. The solution also assumes that at a boundary distance $r = R_b$, modulation of $U(r,T)$ is negligible, and therefore provides the boundary condition at $U(R_b,T) = U_0$ as a known quantity. This quantity, U_0, is ion specific and parametrically described by several free parameters, which are known as Local Interstellar (LIS) parameters.

The analytical solution of the full FP equation exists only for a simple form of κ, and with constant values of $V_s(r)$ and $\alpha(T)$ [13]. Therefore, the FP equation must be solved numerically to obtain flux in the desired

energy range and solar conditions [12]. The solution depends on the assumption that several key quantities are known, including the set of parameters known as Local Inter-stellar (LIS) parameters.

2 Initial parameters and data sets

2.1 Local Interstellar parameters

As described earlier, at a distance well outside of the solar system, the GCR modulation due to the turbulent solar wind and heliospheric magnetic field is negligible. At around $R_b = 100$ AU, it is assumed that each GCR ion energy-flux spectrum is constant. This constant GCR field is referred to as the local interstellar spectrum (j_{ion}) and represents one of the boundary conditions for the BON model. The LIS equation is described with the following parametric model:

$$U_0 \propto \; j_{ion}(T) \mid_{R_b=100\,AU} = j_0 \beta^{\delta} (T + T_0)^{-\gamma} \tag{2}$$

where j_0, δ, and γ are free parameters for each particular GCR ion, and $\beta = v/c$ is the velocity of the ion relative to the speed of the light. The LIS parameters are formulated by using the GCR measurement data from detectors at or near 1 AU, e.g., satellite and balloon measurements. In the model, the flux of any ion beyond nickel (Z > 28) is obtained by scaling from the silicon result.

In this paper, we describe the most recent LIS parameters fitted to an updated data set to improve the BON model. It should be emphasized that all GCR energy spectra (measurements and model) reported in this paper apply to free-space beyond the Earth's magnetosphere.

2.2 Description of the LIS parameters in BON14 model

In this revision of the BON model, we have modified the LIS parameters, j_0, δ, and γ, driven by a sensitivity study by using several metrics. For a detailed description of the sensitivity analysis, please see the referenced publication series by T. Slaba et al. [14–16]. This analysis was completed by dividing ions into charge and energy groups as shown in Table 1.

One of the most distinguishing results of this study was that for the differential effective dose rate as a function of kinetic energy behind 20 g/cm^2 of aluminum shielding at a period of minimal sun activity, the two energy groups between 0.5 GeV/n and 4.0 GeV/n account for most of the exposure for all ions. As seen in the table, for instance, GCR protons and alphas with boundary energy less than 0.5 GeV/n induce approximately 9% of the total effective dose. GCR ions with Z > 2 and boundary energies less than 0.5 GeV/n induce less than 4% of the total effective dose behind 20 g/cm^2 aluminium shielding. Based on the results of this study, the new LIS parameters are fitted to the GCR data.

The measurement database and uncertainty metrics described in T. Slaba et al. [14–16] were implemented and automated. This allowed a range of parameter combinations to be evaluated through the BON model to determine which parameters lead to minimal uncertainties between the model and measurement database for each energy and ion group. A similar procedure, to calibrate free parameters in a simplified empirical GCR model, was previously described and utilized by Matthia et al. [17].

In the BON case, the uncertainty was quantified using average relative difference between data and model, relative uncertainty on effective dose, and χ^2 analysis. Readers are referred to Eqs.[1-6] in T. Slaba et al. [16] for a detailed description of how the relative uncertainty results were incorporated as weighting factors in the analysis.

The computation of the average uncertainty in each energy bin allowed either positive or negative uncertainty values in each bin, which permitted to systematic model trends to be seen (negative values correspond to underprediction, and positive values correspond to overprediction). Whereas the final parameter set for each ion was chosen somewhat subjectively, reduced uncertainty results in the upper, most relevant energy bins were preferred.

Table 1. Relative contributions of the indicated charge groups to effective dose behind 20 g/cm^2 of aluminum shielding at a period of minimal solar activity. The ions were grouped into 5 energy and atomic number categories. Charge groups: Z_1 =1, Z_2 = 2, $Z_3 = 3-10$, $Z_4 = 11-20$, and $Z_5 = 21 - 28$. Kinetic energy groups: $E_1 = 0.0 - 0.25$, $E_2 = 0.25 - 0.5$, $E_3 = 0.5 - 1.5$, $E_4 = 1.5 - 4.0$, and $E_5 = 4.0 - 1.0 \times 10^4$ GeV/n.

Charge \ Energy	$\mathbf{E}_1$	$\mathbf{E}_2$	$\mathbf{E}_3$	$\mathbf{E}_4$	$\mathbf{E}_5$	**Total** [%]
Z_1=1	1.2	5.4	18.2	18.4	14.8	58.1
Z_2=2	1.2	2.2	4.1	2.9	1.7	12.2
Z_3=3 - 10	<0.1	3.3	3.8	1.3	0.8	9.1
Z_4=11 - 20	<0.1	0.2	6.6	2.0	1.1	10.0
Z_5=21 - 28	<0.1	<0.1	4.7	3.8	2.1	10.6
Totals	2.5	11.1	37.4	28.4	20.5	100.0

The LIS parameters for each of the corresponding ions from H to Ni are shown in Table 2.

Table 2. The LIS parameters that are used in the BON14 model shown for each ion.

Z	γ	δ	j_0
1	2.75	-2.82	9.50×10^{-4}
2	2.80	-2.00	4.53×10^{-5}
3	3.21	-0.69	6.37×10^{-8}
4	2.93	1.50	1.20×10^{-7}
5	3.00	-0.40	2.40×10^{-7}
6	2.70	-2.00	1.60×10^{-6}
7	2.95	-0.60	2.65×10^{-7}
8	2.73	-1.90	1.50×10^{-6}
9	3.08	0.40	1.63×10^{-8}
10	2.75	-1.60	2.35×10^{-7}
11	2.73	-1.80	4.60×10^{-8}
12	2.70	-2.40	3.03×10^{-7}
13	2.75	-1.40	5.30×10^{-8}
14	2.65	-2.40	2.65×10^{-7}
15	3.15	2.00	5.68×10^{-9}
16	2.70	-1.00	5.78×10^{-8}
17	3.13	2.00	5.99×10^{-9}
18	2.90	0.60	1.68×10^{-8}
19	3.13	0.80	7.90×10^{-9}
20	2.75	-1.60	3.23×10^{-8}
21	3.15	0.40	3.50×10^{-9}
22	3.00	-0.50	1.44×10^{-8}
23	3.00	-0.50	7.14×10^{-9}
24	2.90	-1.00	1.78×10^{-8}
25	2.80	-1.00	1.39×10^{-8}
26	2.60	-2.40	2.00×10^{-7}
27	2.60	-2.50	1.11×10^{-9}
28	2.55	-2.40	1.19×10^{-8}

2.3 Selection of GCR data

In the past, the BON model parameters were uniquely influenced by measurements from the Cosmic Ray Isotope Spectrometer (CRIS) on the NASA Advanced Composition Explorer (ACE) spacecraft. The CRIS instrument is currently measuring the flux of ions and their isotopes from boron (Z=5) to nickel (Z=28).

Although the lowest and highest kinetic energy measurements are ion specific, the CRIS provides kinetic energy of GCR isotopes between $\sim$ 50 - 500 MeV/n overall. In the BON14 model, greater emphasis was placed on the higher kinetic energies, a region not covered by ACE/CRIS. Nonetheless, we show that the updated model still accurately represents the lower energy regions.

In this revision of the BON model, BON14, we have included the GCR data beyond 1970, which spans Solar Cycle 20 to 24 (to date). Table 3 lists the name, flight type, measurement times, range of GCR ion charge and energy of the measurement data sets that we used for calibrating the LIS parameters.

Table 3. The list of GCR data sets that were used to calibrate the LIS parameters in the BON model. A similar table with more detailed information can be found in [16].

Name	**Flight**	**Time**	**Ions (Z)**	**Energy [GeV/n]**
ACE/CRIS [18]	Satellite	1998 - Present	5 - 28	0.05 - 0.5
AMS [19, 20]	STS-91	1998	1, 2	0.1 - 200.0
ATIC-2 [21]	Balloon	2002	1 - 26†	4.6 - 10.0
BESS [22]	Balloon	1997 - 2000, 2002	1, 2	0.2 - 22.0
CAPRICE [23, 24]	Balloon	1994, 1998	1, 2	0.15 - 350.0
CREAM-II [25]	Balloon	2005	6 - 26†	18.0 - 10.0
HEAO-3 [26]	Satellite	1979	4 - 28	0.62 - 35.0
IMAX [27]	Balloon	1992	1, 2	0.18 - 208.0
IMP-8 [28]	Satellite	1974	6 - 14†	0.05 - 1.0
LEAP [29]	Balloon	1987	1, 2	0.18 - 80.0
MASS [30]	Balloon	1991	1, 2	1.6 - 100.0
PAMELA [31, 32]	Satellite	2006 - 2009	1, 2	0.08 - 10.0
TRACER [33]	Balloon	2003	8 - 26†	0.8 - 10.0
Lezniak et al. [34]	Balloon	1974	4 - 26†	0.35 - 52.0
Minagawa et al. [35]	Balloon	1975	26, 28	1.3 - 10.0
Muller et al. [36]	STS-51	1985	6 - 14†	50.0 - 10.0
Simon et al. [37]	Balloon	1976	5 - 8	2.5 - 10.0

† Not all ion data are available in the provided range.

Most of the GCR data that are collected by the ACE/CRIS instru-

ment have very low count rates, which leads to high statistical measurement errors. There are a few abundant ions with low statistical measurement uncertainty for ions, such as B, C, N, O, and Fe. However, almost all of the ions have very high statistical uncertainty, such as data provided for F, P, Cl, Sc, and most of the heavy ions. Hence, the tables that report the comparison of BON model metrics, multiple successive Bartels rotations were averaged to reduce the statistical uncertainty in the measurements. By doing this, most of the ions have an uncertainty of less than 10% and the highest uncertainty, in this case for Co, was reduced to $\sim 25\%$.

3 Solar modulation

One of the important input parameters of the BON model is the deceleration potential, ϕ, (a.k.a. solar modulation parameter). The deceleration potential is correlated with the diffusion coefficient, κ, and may be used to account for attenuation of the LIS due to the state of the heliosphere. Larger values of ϕ represent lower GCR flux. The ϕ is in units of rigidity (MV), and is proportional to the momentum/charge required for a particle to penetrate the heliosphere. The parametric relation between κ and ϕ can be described by the following equation [38]:

$$\kappa(r,t) = \frac{\kappa_0}{V_s}\beta P[1 + (\frac{r}{r_0})^2]/\phi(t) \tag{3}$$

where V_s is the constant solar wind speed ($\sim$ 400 km/s), r is distance from the Sun in AU, t is time in years, κ_0 is a diffusion constant (1.6×10^{21} cm^2/s), and P is particle rigidity in units of MV. In order to fit ions from H to Ni by using a simple form of the LIS model, r_0 is arbitrarily set to 4.0 AU [38]. It is important to note that the value of κ_0 is chosen somewhat arbitrarily, therefore the values of $\phi(t)$ are not significant. They simply define the level of modulation for a given period of time within the context of our choice of parameters. In Fig. 1, GCR data for various ions for low- and high-solar activity times are shown. The solar modulation is very noticeable for energies lower than $\sim$ 4 GeV/n for H and He.

Methods that determine ϕ from the current measurement of solar activity at the Sun, such as sunspot number, show a lag of the GCR modulation. The BON model incorporates a time-delay function [39] to account for the lag because of Solar effects which take a certain amount of time ($\sim 8-14$ months) to reach the boundary of the heliosphere. In addition, the magnetic polarity reversal of the Sun is considered by the model.

On the other hand, direct measurement of the GCR flux by a spacecraft instrument samples the current state of the heliosphere. The sunspot method has the advantage of predicting future GCR fluxes; however, the spacecraft method can more directly sample the actual GCR flux.

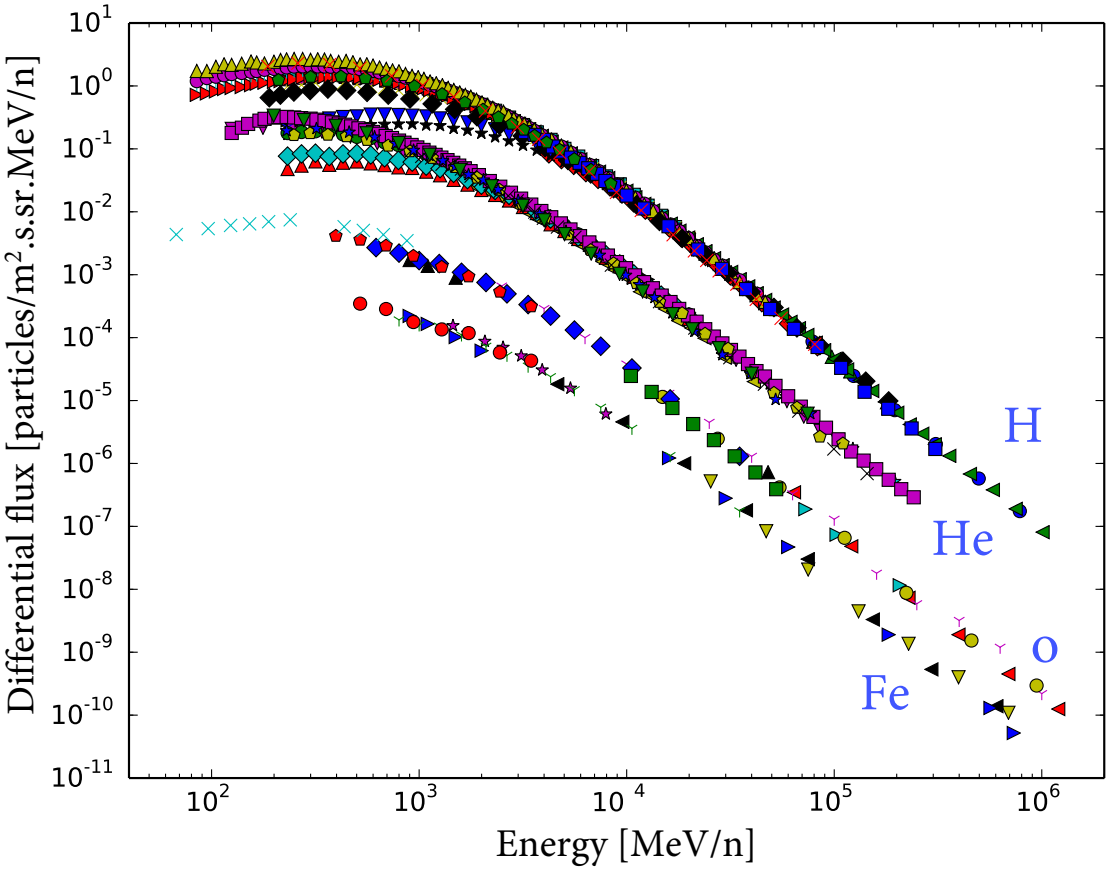

Figure 1. The flux data as a function of kinetic energy for H, He, O, and Fe are shown for all the data used for calibration (this plot excludes ACE/CRIS data).

In Fig. 2, the ϕ computed by using BON14 and monthly smoothed average international sunspot number (SSN) [40] as a function of time are shown. The left axis represents the SSN and the right axis represents the ϕ. The figure clearly presents the time-delay effect incorporated in the ϕ, where ϕ is calculated from the SSN by accounting for the time-delay between the time of the solar activity (the sunspots) and the time this effect (the magnetic field disturbance) reaches into the heliosphere enough to significantly modulate the GCR flux.

In this current revision of the BON model, as opposed to the previous BON11 model [9] where there were two ϕ values (one for the proton and another ϕ for all other ions); there is only one ϕ input for all of the ions. A single value of ϕ describes the state of the heliosphere at a given time and is used for all elements from hydrogen (Z=1) through plutonium (Z=94).

Analysis shows that the correlation of the spectra of all the significant

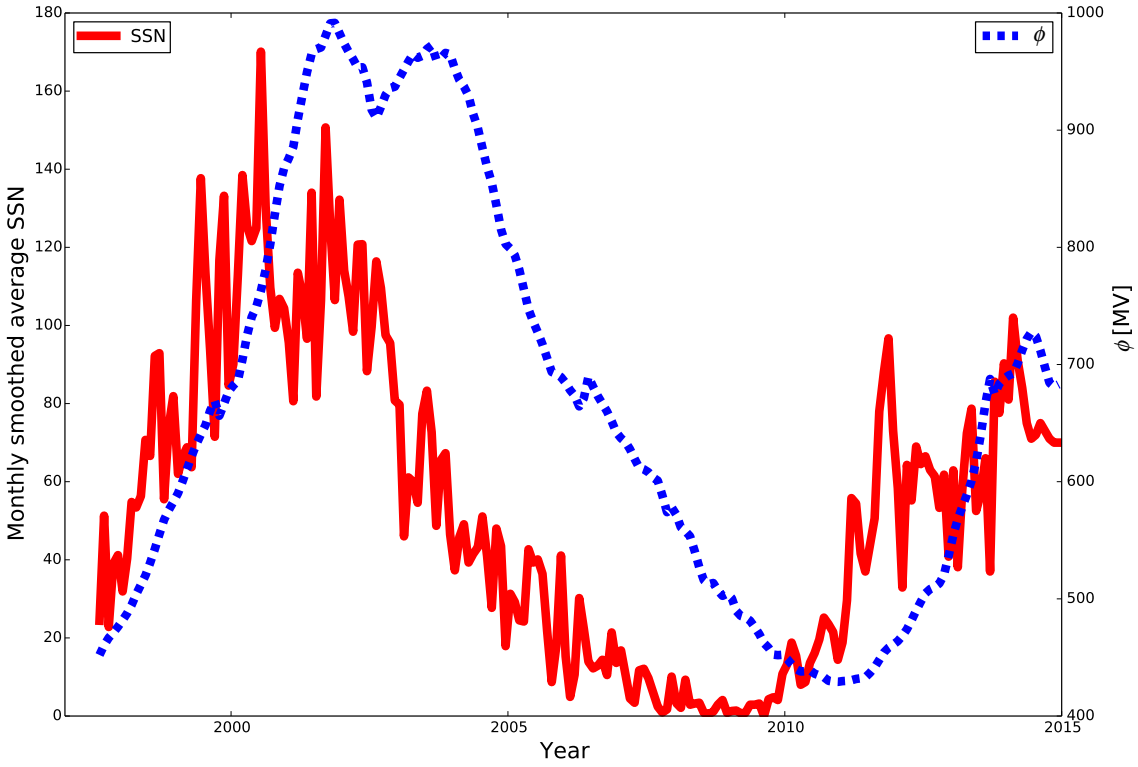

Figure 2. The monthly smoothed average SSN and ϕ (deceleration potential) as a function of time for the period between 1998-2015 are shown. On the left axis SSN (red solid line) and on the right axis ϕ (blue dashed line) are shown. The ϕ function is shifted in time due to the time-delay function.

GCR elements (Z=1 to 28) is better when using direct sampling of the heliosphere by spacecraft to determine the ϕ. This is important to the SEE analyst who needs to know the actual history of GCR fluxes, where the SEE analyst needs knowledge of actual worst-case conditions for spacecraft designs.

It is worth noting here that the ϕ is directly associated with solar activity and can be determined (in principle) by a number of methods. The various solar indices - e.g., sunspot number, radio and X-ray flux, neutron monitor rates, spacecraft GCR measurements, and even tree growth rings - indicate the temporal variation of the Sun's intensity.

4 Comparison of the BON14 model to the data

The comparison of the BON14 model with the GCR measurement data (GCR database provided in Table 1) was done by using several metrics as explained in Sec. 2.2. That included looking at relative differences, analyzing distributions of uncertainties, and inclusion of measurement

uncertainty. It is worth mentioning here that since almost all of the GCR measurement are broadly binned (with error bars), we integrated the BON model output data to match the same energy bin of the measurement data and considered the average of the points. No significant differences were found if comparisons were done using the data midpoints instead.

The relative difference, Rd, is a measurement between the GCR measurement data and the BON model that allows us to find where the model underpredicts or overpredicts the measured GCR flux. Rd is shown as:

$$Rd = \frac{1}{N}\sum_{k=1}^{N}\frac{Model_k - Data_k}{Data_k}, \tag{4}$$

where N is the number of measurements. The average of the residual Rd does not provide a complete picture of the model versus measurement agreement, as the quantity may end up in the vicinity of zero due to positive-negative cancellation effect, yet the uncertainty may still be high. Therefore, we also used the average absolute relative difference, $|Rd|$, to determine the overall difference between the model and the GCR measurement data, which can be described as:

$$|Rd| = \frac{1}{N}\sum_{k=1}^{N}\frac{|Model_k - Data_k|}{Data_k} \tag{5}$$

This metric better quantifies the spread in model errors and may be used as a quality check for the model. In addition to the nominal data measurement comparison metrics, we extended our uncertainty analysis by including a measure of fit relative to the error bars described as following:

$$\begin{aligned} U_{lower} &= \frac{1}{N}\sum_{k=1}^{N}\frac{Model_k - [Data_k - \varepsilon_k^-]}{Data_k - \varepsilon_k^-}, \\ U_{upper} &= \frac{1}{N}\sum_{k=1}^{N}\frac{Model_k - [Data_k + \varepsilon_k^+]}{Data_k + \varepsilon_k^+}, \end{aligned} \tag{6}$$

where ε^- and ε^+ are published lower and upper error bars on data, respectively, and U_{lower} and U_{upper} represent the uncertainty interval that incorporates the GCR data measurement error bars. The width of the interval is approximately considered as the measurement uncertainty. In Fig. 3, the comparison of uncertainty metrics between the GCR measurement database presented in Table 3 and BON10 [8], BON11, and BON14 models are shown as functions of energy and charge groups. As clearly seen from the figure, there is a noticeable improvement with BON14 in almost every bin over BON10 and BON11. The improvement is especially significant for ions in the important energy bins between 0.5 and

4.0 GeV/n. As shown in Table 1, based on the sensitivity study, about 66% of the total effective dose is induced by the ions within this energy range. Thus, more emphasis was placed on minimizing the uncertainty in those bins.

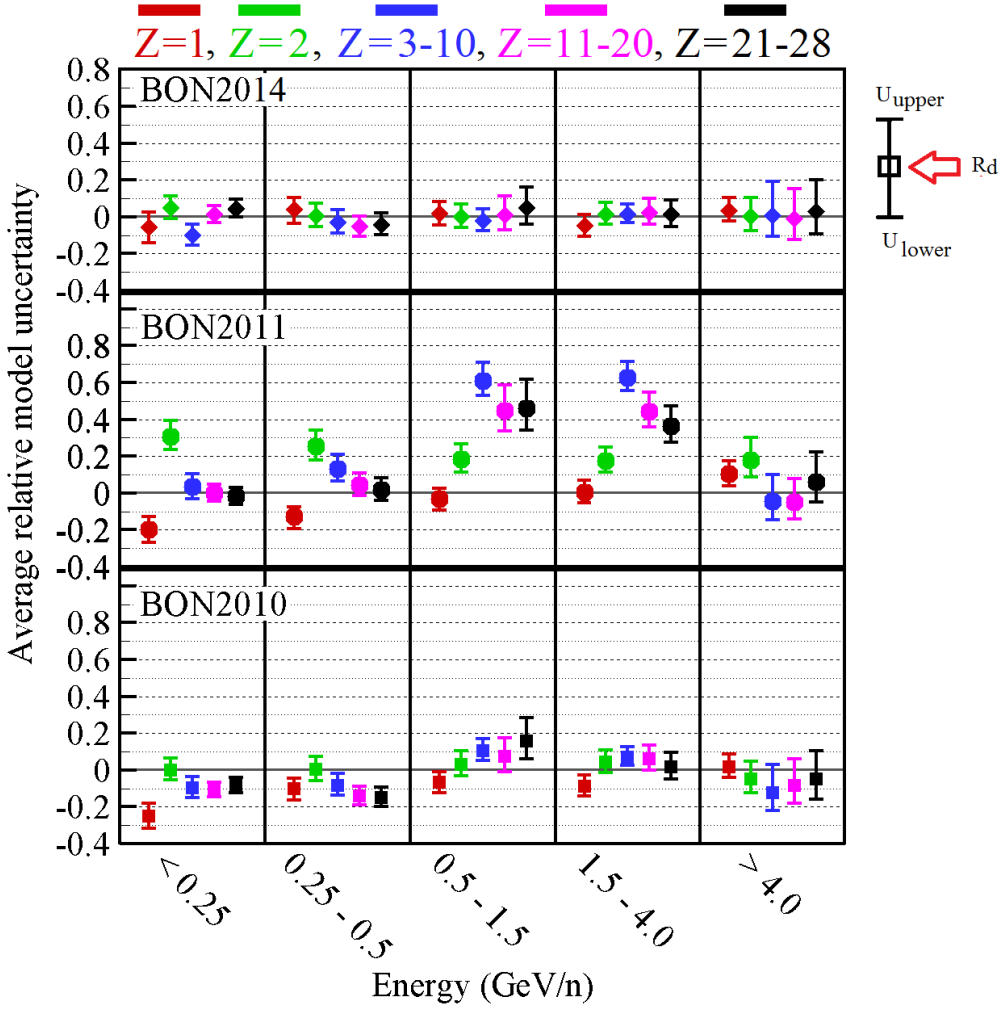

Figure 3. The average relative model uncertainty as a function of charge and energy groups are shown for BON10, BON11, and BON14 models. As illustrated on the right side of the figure, the marker positions represent Rd, while error bars represent upper and lower uncertainty interval.

Figures 4−7 show the comparison of the average of the integrated differential flux for H, He, O, and Fe for each data set with BON11 and BON14 models. In these figures, we separated the data into two energy regions to simplify comparisons. The top plots represent lower energy bins ($<$ 4.0 GeV/n) and bottom plots represent higher energy bins ($\geq$ 4.0 GeV/n). We define the average flux ($< U >$) as the integral of the differential flux (dU/dE) over all energy bins, which is given by the

following equation:

$$< U >= \frac{1}{N_{bin}} \int \frac{dU}{dE} dE, \tag{7}$$

where N_{bin} is the number of energy bins and dE is the bin width of the data set. Average flux was evaluated by summing over the reported energy bins. The $|Rd|$ values for low-energy for H ion are 18.7% and 13.6% for BON11 and BON14 models, respectively. Moreover, as shown in the Fig. 5 for He, Fig. 6 for O, and Fig. 7 for Fe, the BON14 model presents a significant improvement over the BON11 model especially for energies below 4.0 GeV/n.

In Fig. 8 *Rd* comparisons between ACE/CRIS data with the BON11 model (top) and BON14 model (bottom) were plotted for O [at a recommended] mid-energy of 230.8 MeV/n. The left axis on this figure presents the GCR measurement data and BON model differential fluxes in units of particles/s·sr·m^2·MeV/n. The right axis shows average *Rd* for each data set. The $|Rd|$ for BON14 is about a factor of 2 lower than BON11; where it was calculated as 26% for BON11 and 13.6% for BO14 for the oxygen GCR data between 1998 - 2014 (August through December, 1997 data were not included in the validation due to issues with data calibration as reported in [41]).

As discussed in Sec. 2, greater emphasis was placed on higher kinetic energies, which is not covered by the ACE/CRIS model. Although the new model still has large relative difference during solar maximum periods ($\sim 2000 - 2005$), we present that BON14 has been significantly improved over the BON11 version. Moreover, BON14 follows the oxygen GCR data better for the solar activity period between 2010 and 2015.

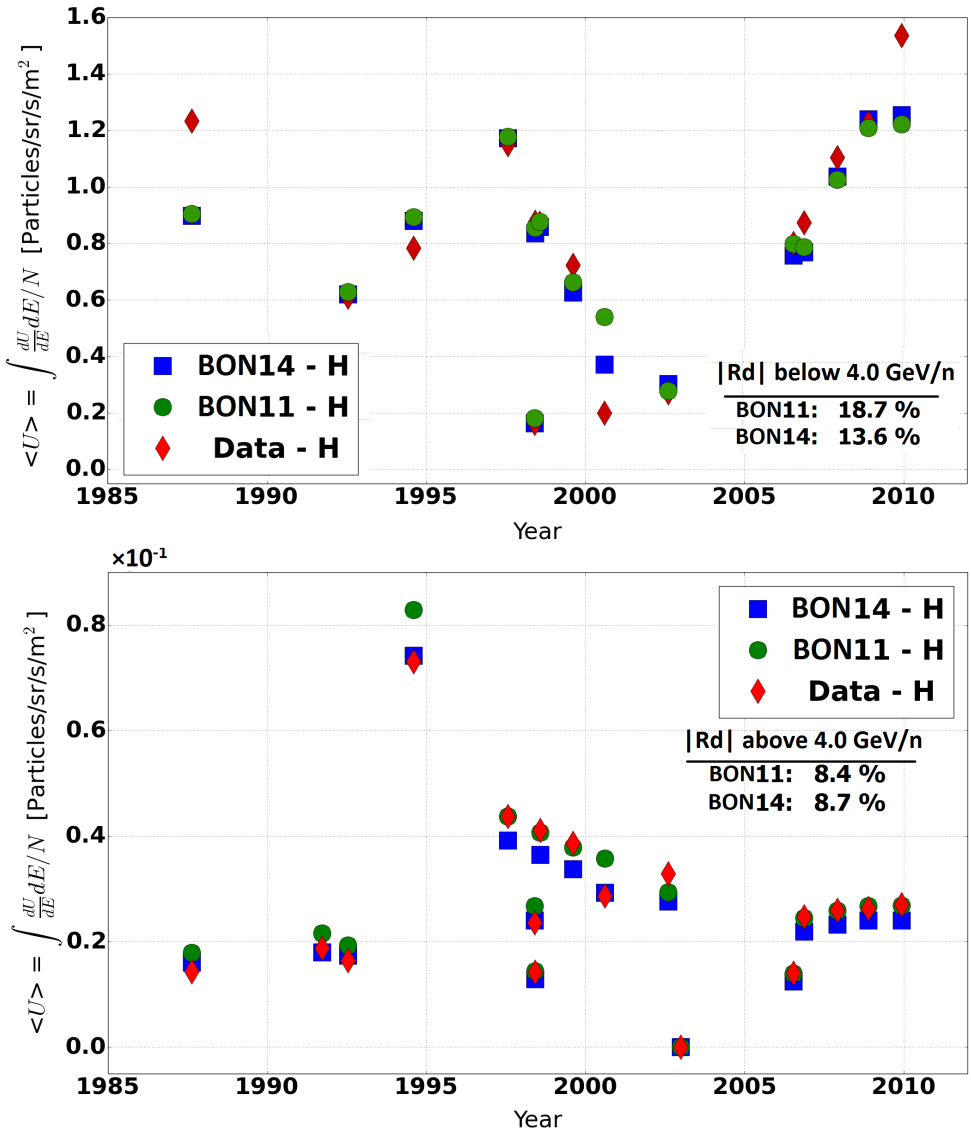

Figure 4. The average flux for H ions as a function of measurement date is shown for BON11 and BON14 models for low-energy (top) and high-energy (bottom).

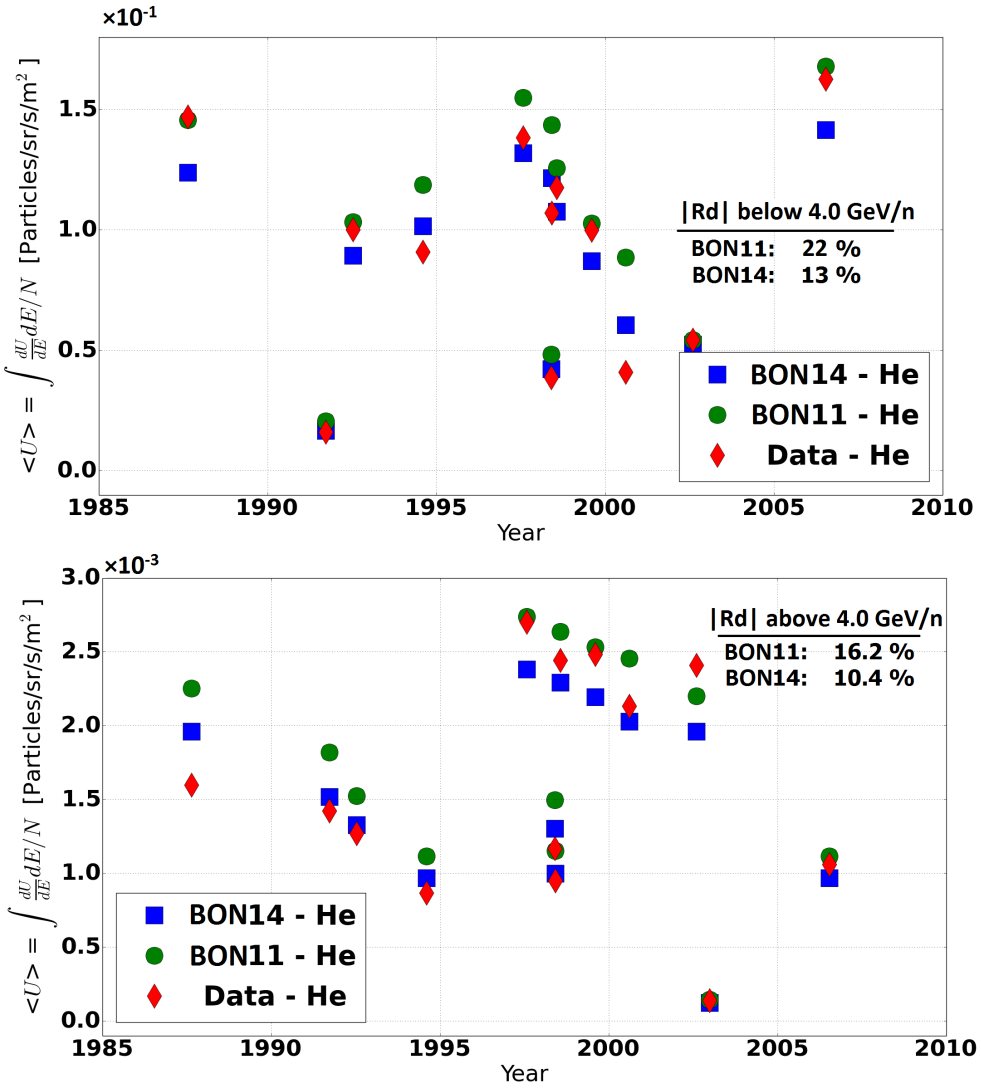

Figure 5. The average flux for He ions as a function of measurement date is shown for BON11 and BON14 models for low-energy (top) and high-energy (bottom).

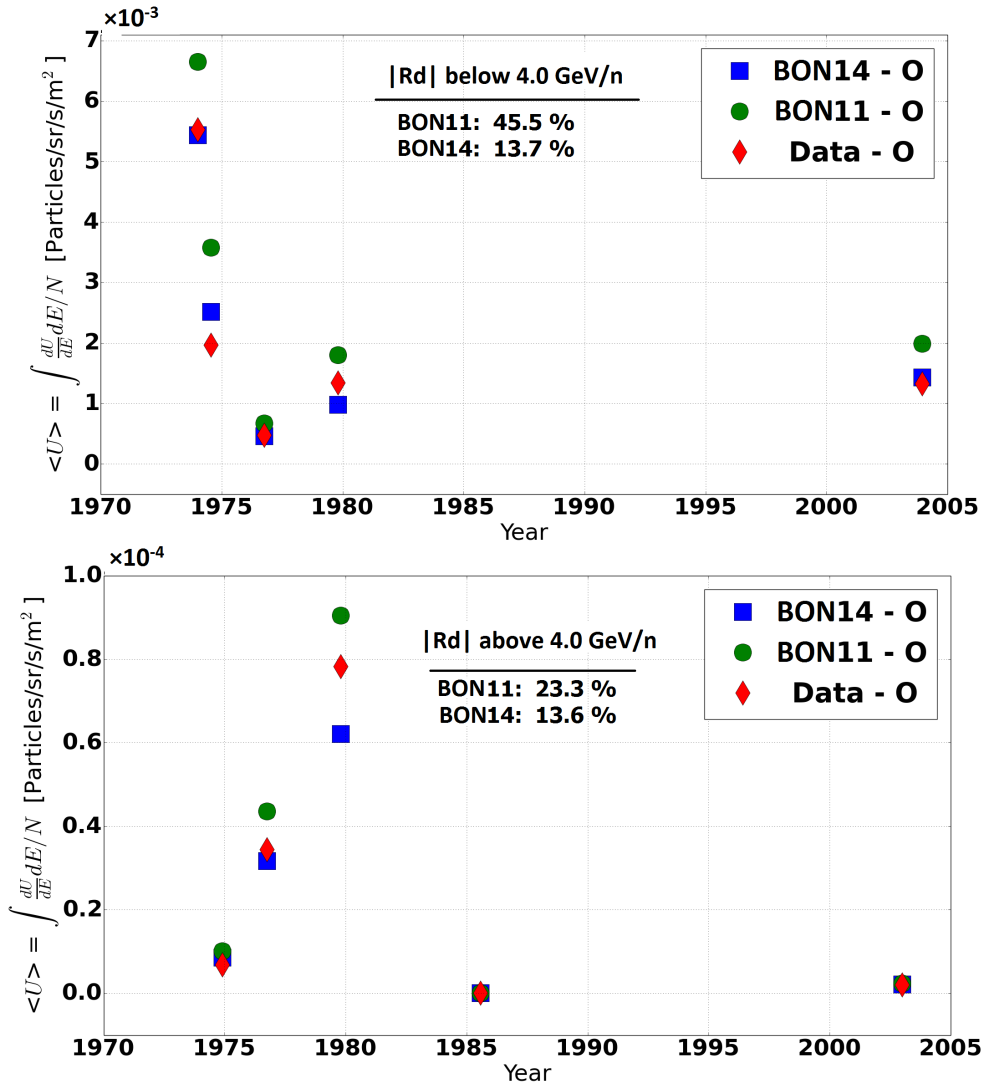

Figure 6. The average flux for O ions as a function of measurement time is shown for BON11 and BON14 models for low-energy (top) and high-energy (bottom). Note that this plot does not include data from ACE/CRIS.

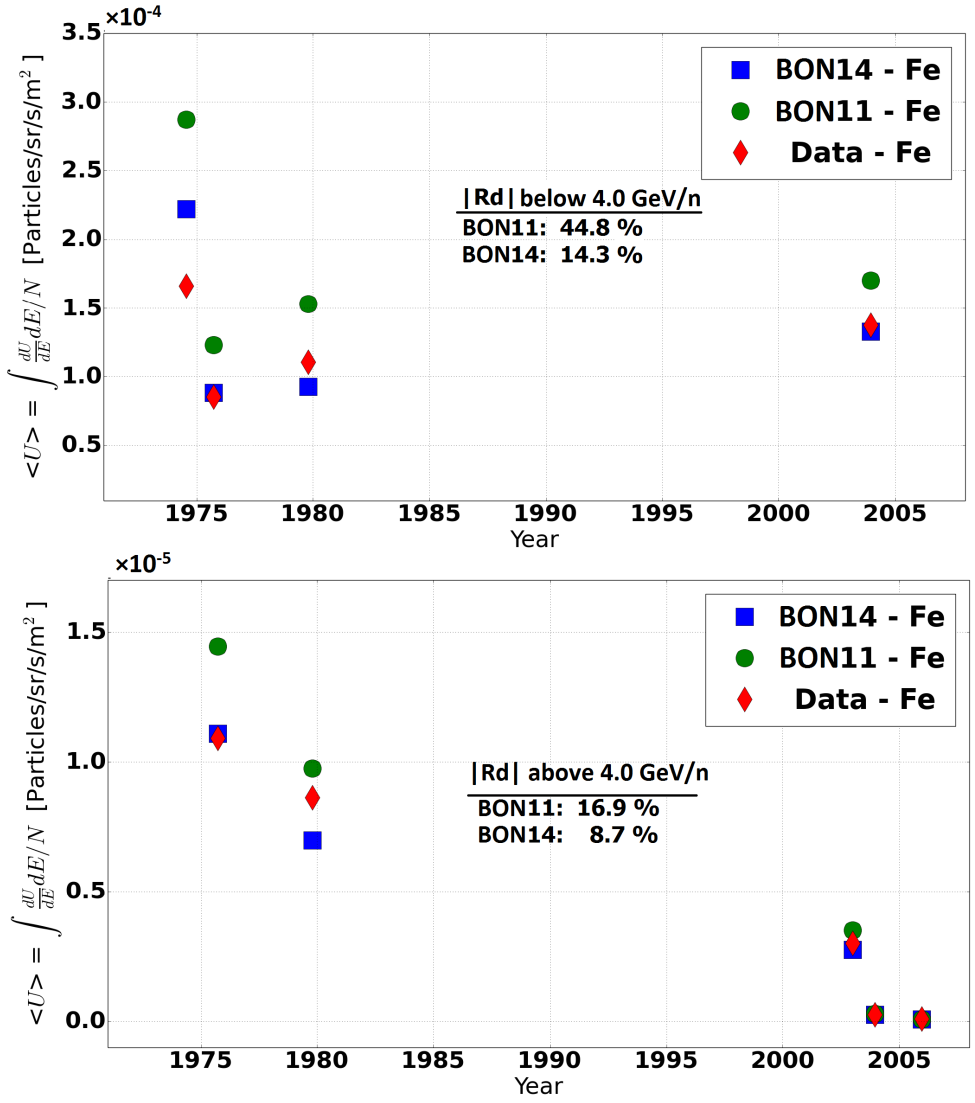

Figure 7. The average flux for Fe ions as a function of measurement time is shown for BON11 and BON14 models for low-energy (top) and high-energy (bottom). Note that this plot does not include data from ACE/CRIS.

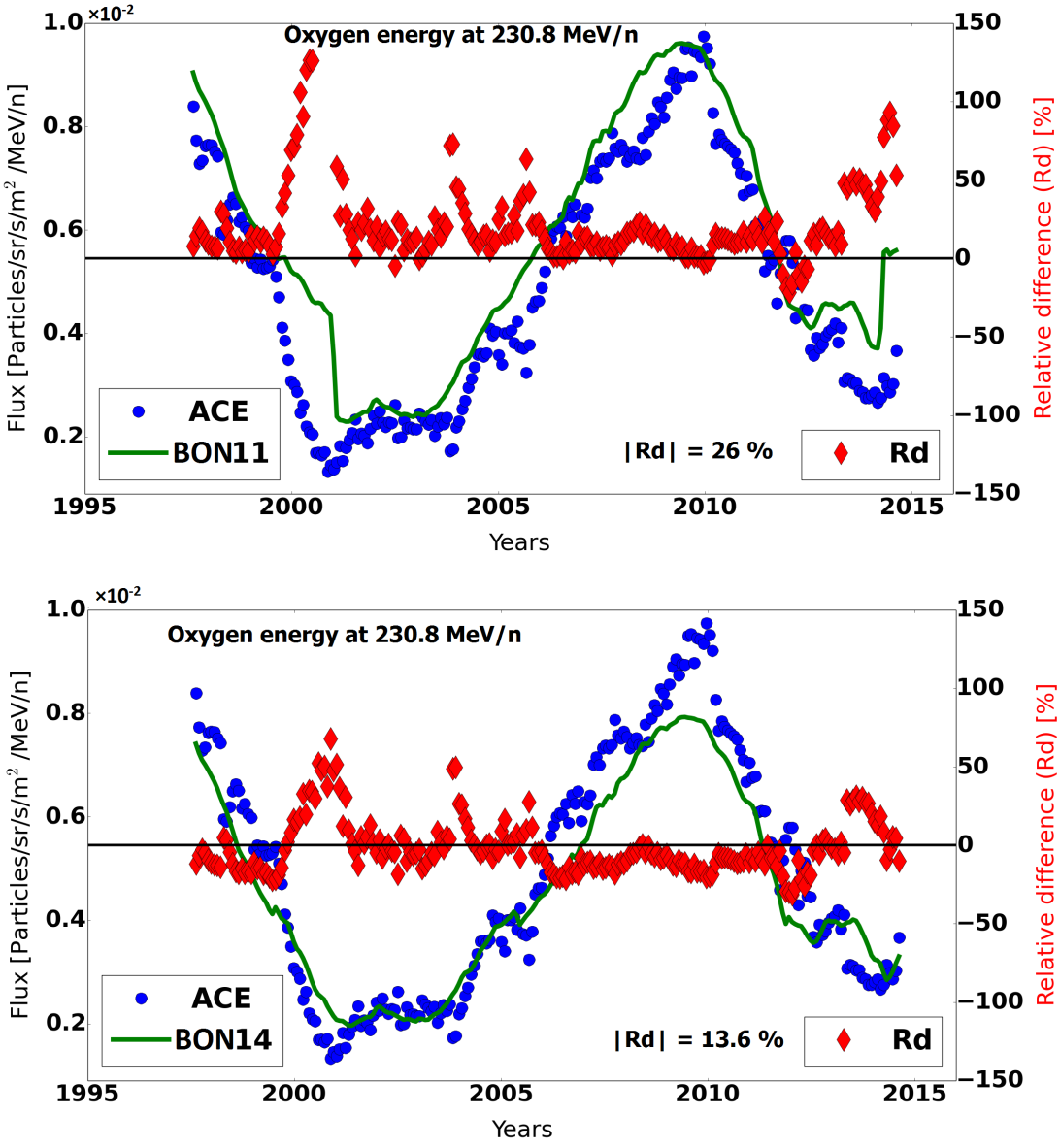

Figure 8. The ACE/CRIS flux data as a function of Bartels'-rotation (27-day average) from 1998-present for O ion is compared with (top) BON11 model and (bottom) BON14 model. The axis on the right represents *Rd* between the BON model and GCR data.

In Table 4, the overall average relative difference metrics, Rd and $|Rd|$, are presented for the BON11 and BON14 models. These values were determined by averaging the relative difference metrics over each ion, as given in Appendix A. The results in Appendix A were obtained by considering the entire GCR measurement database (all ion and energy bins). It is seen in Table 4 (and Appendix A), that for BON11, the $|Rd|$ value is calculated as 23.7% and $Rd = 17.9\%$. For BON14, these errors are reduced to $|Rd| = 13.0\%$ and $Rd = -0.4\%$. The BON11 model systematically overpredicts the GCR measurement data, whereas the new BON14 model provides a more balanced prediction. More importantly, the overall spread in the new model error was reduced from 23.7% to 13.0%. It should be emphasized that at all energies, BON14 is only a marginally improved fit to the hydrogen GCR data compared with BON11. There is room for improvement since BON14 underpredicts the hydrogen GCR data during $\sim$ 8 years since 1998 (per lower panel of Fig. 4). A similar underpredicting pattern is observed for He as well.

Table 4. The average relative difference metrics between the entire GCR database with BON11 and BON14.

All GCR measurement data		
	Average [%]	
	Rd	$\|Rd\|$
BON11	17.9	23.7
BON14	-0.4	13.0

5 Conclusions

Presented are the new methodology to obtain the LIS parameters and comparison of the results of the new BON14 model with a new set of GCR data from various balloon, satellite, and space shuttle measurements. The sensitivity study described earlier showed that the two energy groups between 0.5 GeV/n and 4.0 GeV/n account for most of the shielded effective dose for all ions. Therefore, we modified the LIS parameters, j_0, δ, and γ, driven by this sensitivity study.

The overall average Rd value is calculated as 17.9% for the BON11 and -0.4% for the BON14 model, whereas $|Rd|$ is found as 23.7% and 13.0% for BON11 and BON14 models, respectively. The uncertainty metrics for 5 energy bins and charge groups also revealed that overall the BON14 model has been improved significantly with respect to the previous models both at low- and high-energy regions. The new model especially provides less uncertainty for ions in the important energy bins

between 0.5 and 4.0 GeV/n, which account for a significant part of the total effective dose behind shielding. However, it should be noted that the LIS parameters used by BON14 slightly underpredict hydrogen GCR data for most of the years since $\sim$ 1998 (beginning of a solar maximum). Following the release of the BON14 model, we will attempt to improve the model by incorporating several physics effects on the GCR particles (e.g., curvature and gradient drifts) which have not been included in the previous BON models.

References

1. "National Council on Radiation Protection and Measurements (NCRP), Information Needed to Make Radiation Protection Recommendations for Space Missions Beyond Low-Earth Orbit," Tech. Rep. No. 153, Natl. Counc. on Radiat. Prot. and Meas., Bethesda, Maryland, 2006.

2. F. A. Cucinotta, M.-H. Y. Kim, and L. J. Chappell, "Space Radiation Cancer Risk Projections and Uncertainties 2012," Tech. Rep. NASA/TP-2013-217375, (2013).

3. M. Durante and F. A. Cucinotta, "Physical basis of radiation protection in space travel," *Rev. Mod. Phys.*, vol. 83, pp. 1245–1281, Nov 2011.

4. L. Adams, "Cosmic ray effects in microelectronics," *Microelectronics Journal*, vol. 16, no. 2, pp. 17 – 29, 1985.

5. P. M. O'Neill and G. D. Badhwar, "Single event upsets for Space Shuttle flights of new general purpose computer memory devices," *IEEE Transactions on Nuclear Science*, vol. 41, pp. 1755–1764, Oct. 1994.

6. G. D. Badhwar and P. M. O'Neill, "Long-term modulation of galactic cosmic radiation and its model for space exploration.," *Advances in Space Research*, vol. 14, no. 10, pp. 749 – 757, 1994.

7. G. Badhwar and P. O'Neill, "Galactic cosmic radiation model and its applications," *Advances in Space Research*, vol. 17, no. 2, pp. 7 – 17, 1996.

8. P. O'Neill, "Badhwar-O'Neill 2010 Galactic Cosmic Ray Flux Model; Revised," *Nuclear Science, IEEE Transactions on*, vol. 57, pp. 3148–3153, Dec 2010.

9. P. M. O'Neill and C. C. Foster, "Badhwar-ONeill 2011 Galactic Cosmic Ray Flux Model Description," Tech. Rep. NASA/TP-2013-217376, (2013).

10. E. N. Parker, "The passage of energetic charged particles through interplanetary space," *Planetary and Space Science*, vol. 13, no. 1, pp. 9 – 49, 1965.

11. L. J. Gleeson and W. I. Axford, "Cosmic rays in the interplanetary medium," *Astrophysical Journal*, vol. 149, p. L115, 1967.

12. L. A. Fisk, "Solar modulation of galactic cosmic rays, 2," *Journal of Geophysical Research*, vol. 76, no. 1, pp. 221–226, 1971.

13. L. A. Fisk and W. I. Axford, "Solar modulation of galactic cosmic rays, 1," *Journal of Geophysical Research*, vol. 74, no. 21, pp. 4973 – 4986, 1969.

14. T. C. Slaba and S. R. Blattnig, "GCR environmental models I: Sensitivity analysis for GCR environments," *Space Weather*, vol. 12, no. 4, pp. 217–224, 2014.

15. T. C. Slaba and S. R. Blattnig, "GCR environmental models II: Uncertainty propagation methods for GCR environments," *Space Weather*, vol. 12, no. 4, pp. 225–232, 2014.

16. T. C. Slaba, X. Xu, S. R. Blattnig, and R. B. Norman, "GCR environmental models III: GCR model validation and propagated uncertainties in effective dose," *Space Weather*, vol. 12, no. 4, pp. 233–245, 2014.

17. D. Matthi, T. Berger, A. I. Mrigakshi, and G. Reitz, "A ready-to-use galactic cosmic ray model," *Advances in Space Research*, vol. 51, no. 3, pp. 329 – 338, 2013.

18. E. C. Stone, A. M. Frandsen, R. A. Mewaldt, E. R. Christian, D. Margolies, J. F. Ormes, and F. Snow, "The advanced composition explorer," *Space Science Reviews*, vol. 86, no. 1-4, pp. 1–22, 1998.

19. J. Alcaraz et al., "Cosmic protons," *Physics Letters B*, vol. 490, no. 12, pp. 27 – 35, 2000.

20. J. Alcaraz et al., "Helium in near earth orbit," *Physics Letters B*, vol. 494, no. 34, pp. 193 – 202, 2000.

21. A. D. Panov et al., "Energy spectra of abundant nuclei of primary cosmic rays from the data of ATIC-2 experiment: Final results," *Bulletin of the Russian Academy of Sciences: Physics*, vol. 73, no. 5, pp. 564–567, 2009.

22. Y. Shikaze et al., "Measurements of 0.220 GeV/n cosmic-ray proton and helium spectra from 1997 through 2002 with the BESS spectrometer," *Astroparticle Physics*, vol. 28, no. 1, pp. 154 – 167, 2007.

23. M. Boezio et al., "The Cosmic-Ray Proton and Helium Spectra between 0.4 and 200 GV," *The Astrophysical Journal*, vol. 518, pp. 457–472, June 1999.

24. M. Boezio et al., "The cosmic-ray proton and helium spectra measured with the CAPRICE98 balloon experiment," *Astroparticle Physics*, vol. 19, pp. 583–604, Aug. 2003.

25. H. S. Ahn et al., "Energy Spectra of Cosmic-ray Nuclei at High Energies," *The Astrophysical Journal*, vol. 707, pp. 593–603, Dec. 2009.

26. J. J. Engelmann, P. Ferrando, A. Soutoul, P. Goret, and E. Juliusson, "Charge composition and energy spectra of cosmic-ray nuclei for elements from Be to NI - Results from HEAO-3-C2," *Astronomy and Astrophysics*, vol. 233, pp. 96–111, July 1990.

27. W. Menn et al., "The Absolute Flux of Protons and Helium at the Top of the Atmosphere Using IMAX," *The Astrophysical Journal*, vol. 533, pp. 281–297, Apr. 2000.

28. M. Garcia-Munoz, G. M. Mason, J. A. Simpson, and J. P. Wefel, "Charge and energy spectra of heavy cosmic rays at intermediate energies," *International Cosmic Ray Conference*, vol. 1, pp. 230–235, 1977.

29. E. S. Seo, J. F. Ormes, R. E. Streitmatter, S. J. Stochaj, W. V. Jones, S. A. Stephens, and T. Bowen, "Cosmic Ray Proton and Helium Spectra During the 1987 Solar Minimum," *International Cosmic Ray Conference*, vol. 1, p. 627, Aug. 1991.

30. R. Bellotti et al., "Balloon measurements of cosmic ray muon spectra in the atmosphere along with those of primary protons and helium nuclei over midlatitude," *Phys. Rev. D*, vol. 60, p. 052002, Jul 1999.

31. O. Adriani et al., "PAMELA Measurements of Cosmic-Ray Proton and Helium Spectra," *Science*, vol. 332, p. 69, Apr. 2011.

32. O. Adriani et al., "Time Dependence of the Proton Flux Measured by PAMELA during the 2006 July-2009 December Solar Minimum," *The Astrophysical Journal*, vol. 765, p. 91, Mar. 2013.

33. M. Ave, P. J. Boyle, F. Gahbauer, C. Höppner, J. R. Hörandel, M. Ichimura, D. Müller, and A. Romero-Wolf, "Composition of Primary Cosmic-Ray Nuclei at High Energies," *The Astrophysical Journal*, vol. 678, pp. 262–273, May 2008.

34. J. A. Lezniak and W. R. Webber, "The charge composition and energy spectra of cosmic-ray nuclei from 3000 MeV per nucleon to 50 GeV per nucleon," *The Astrophysical Journal*, vol. 223, pp. 676–696, July 1978.

35. G. Minagawa, "The abundances and energy spectra of cosmic ray iron and nickel at energies from 1 to 10 GeV per AMU," *The Astrophysical Journal*, vol. 248, pp. 847–855, Sept. 1981.

36. D. Mueller, S. P. Swordy, P. Meyer, J. L'Heureux, and J. M. Grunsfeld, "Energy spectra and composition of primary cosmic rays," *The Astrophysical Journal*, vol. 374, pp. 356–365, June 1991.

37. M. Simon, H. Spiegelhauer, W. K. H. Schmidt, F. Siohan, J. F. Ormes, V. K. Balasubrahmanyan, and J. F. Arens, "Energy spectra of cosmic-ray nuclei to above 100 GeV per nucleon," *The Astrophysical Journal*, vol. 239, pp. 712–724, July 1980.

38. P. M. O'Neill, "Badhwar-O'Neill galactic cosmic ray model update based on advanced composition explorer (ACE) energy spectra from 1997 to present," *Advances in Space Research*, vol. 37, no. 9, pp. 1727 – 1733, 2006.

39. R. A. Nymmik, "Time lag of galactic cosmic ray modulation: conformity to general regularities and influence on particle energy spectra," *Advances in Space Research*, vol. 26, no. 11, pp. 1875 – 1878, 2000.

40. "Source: WDC-SILSO, Royal Observatory of Belgium, Brussels," (accessed February 6, 2015). http://sidc.oma.be/silso/datafiles.

41. "ACE/CRIS database, 2013," (Info released on: January 23, 2013). http://www.srl.caltech.edu/ACE/ASC/level2/lvl2DATA_CRIS.html.

Appendix A

The average relative difference metrics

Table A5. The comparison of the metrics between the entire GCR database with BON11 and BON14 for each ion.

	BON11				BON14			
	ACE/CRIS		Others		ACE/CRIS		Others	
Z	Rd	$\|Rd\|$	Rd	$\|Rd\|$	Rd	$\|Rd\|$	Rd	$\|Rd\|$
1	-	-	7.5	13.6	-	-	-1.6	11.1
2	-	-	18.3	19.1	-	-	0.3	11.7
3	-	-	-	-	-	-	-	-
4	-	-	61.5	61.5	-	-	-7.3	20.1
5	22.3	24.4	46.0	46.0	1.3	11.1	-1.5	16.1
6	21.3	23.6	27.1	34.2	-2.1	12.7	0.0	15.6
7	21.4	23.3	32.8	35.0	-5.0	12.7	1.4	35.8
8	17.0	20.6	28.6	34.4	-3.1	12.8	-0.3	13.7
9	14.3	18.5	24.3	24.3	8.6	13.0	-12.4	14.8
10	15.1	17.9	16.4	30.9	2.9	11.4	-3.3	13.5
11	13.8	17.9	40.9	40.9	3.1	12.1	-7.5	24.1
12	16.6	18.7	22.9	31.7	5.5	12.6	-1.7	17.1
13	14.2	17.3	33.8	33.8	6.9	12.5	-3.6	16.9
14	14.4	17.2	26.0	29.4	2.9	12.2	-2.0	16.8
15	6.6	16.2	19.8	19.8	7.8	15.1	-4.3	4.3
16	11.0	14.9	15.1	24.7	3.3	11.8	-5.0	12.2
17	2.5	14.2	22.5	22.5	3.9	11.7	-1.3	3.0
18	5.7	13.6	-3.0	18.5	3.2	11.9	-6.3	12.4
19	-0.6	13.6	16.1	16.1	10.0	14.0	-2.5	2.5
20	-0.5	14.2	20.2	20.2	-9.5	15.2	-0.1	15.3
21	-5.9	16.0	17.1	17.1	6.6	13.7	2.3	4.3
22	4.5	13.0	25.5	25.5	-1.9	11.7	1.7	3.9
23	2.2	13.8	23.3	23.3	5.5	12.2	2.6	2.9
24	5.6	13.5	19.9	19.9	6.9	12.9	-2.5	2.5
25	8.7	15.1	33.5	33.5	-0.1	12.9	-2.1	2.5
26	7.1	12.1	28.5	30.9	-1.9	12.5	-1.6	11.5
27	-11.1	36.8	2.9	15.7	10.1	34.0	-14.3	14.3
28	2.7	14.2	44.4	44.4	-2.7	13.4	-0.4	12.2
Average	8.7	17.5	24.9	28.4	2.6	13.6	-2.7	12.3

Table A6. The comparison of the metrics between entire GCR data (ACE/CRIS and Others) with BON11 for each ion. The comparison presented here is separated into low-energy (< 4.0 GeV/n) and high-energy (≥ 4.0 GeV/n) regions. The average relative difference is averaged over the results of all the ions.

BON11								
	ACE/CRIS		Others				All GCR Data	
	Low-energy		Low-energy		High-energy		All energies	
Z	Rd	$\|Rd\|$	Rd	$\|Rd\|$	Rd	$\|Rd\|$	Rd	$\|Rd\|$
1	-	-	8.6	18.7	6.5	8.4	7.5	13.6
2	-	-	21.8	22.0	14.9	16.2	18.3	19.1
3	-	-	-	-	-	-	-	-
4	-	-	103.9	103.9	19.1	19.1	61.5	61.5
5	22.3	24.4	63.4	63.4	28.5	28.5	34.1	35.2
6	21.3	23.6	44.4	44.4	9.8	24.1	24.2	28.9
7	21.4	23.3	37.9	37.9	27.7	32.1	27.1	29.1
8	17.0	20.6	45.5	45.5	11.6	23.3	22.8	27.5
9	14.3	18.5	31.5	31.5	17.0	17.0	19.3	21.4
10	15.1	17.9	42.8	42.8	-10.0	19.1	15.7	24.4
11	13.8	17.9	67.9	67.9	14.0	14.0	27.3	29.4
12	16.6	18.7	46.7	46.7	-0.8	16.6	19.7	25.2
13	14.2	17.3	49.9	49.9	17.6	17.6	24.0	25.5
14	14.4	17.2	49.7	49.7	2.3	9.2	20.2	23.3
15	6.6	16.2	19.7	19.7	19.9	19.9	13.2	18.0
16	11.0	14.9	30.1	30.1	0.2	19.3	13.0	19.8
17	2.5	14.2	25.9	25.9	19.1	19.1	12.5	18.3
18	5.7	13.6	0.4	14.0	-6.4	23.0	1.3	16.0
19	-0.6	13.6	19.4	19.4	12.9	12.9	7.7	14.8
20	-0.5	14.2	30.3	30.3	10.1	10.1	9.8	17.2
21	-5.9	16.0	15.0	15.0	19.2	19.2	5.6	16.5
22	4.5	13.0	32.4	32.4	18.5	18.5	15.0	19.2
23	2.2	13.8	35.5	35.5	11.2	11.2	12.8	18.6
24	5.6	13.5	28.5	28.5	11.3	11.3	12.7	16.7
25	8.7	15.1	47.6	47.6	19.4	19.4	21.1	24.3
26	7.1	12.1	44.8	44.8	12.2	16.9	17.8	21.5
27	-11.1	36.8	18.6	18.6	-12.9	12.9	-4.1	26.3
28	2.7	14.2	61.7	61.7	27.0	27.0	23.6	29.3
Average	8.7	17.5	37.9	38.8	11.8	18.0	17.9	23.7

Table A7. The comparison of the metrics between entire GCR data (ACE/CRIS and Others) with BON14 for each ion. The comparison presented here is separated into low-energy (< 4.0 GeV/n) and high-energy (≥ 4.0 GeV/n) regions. The average relative difference is averaged over the results of all the ions.

BON14								
	ACE/CRIS		Others				All GCR Data	
	Low-energy		Low-energy		High-energy		All energies	
Z	Rd	$\|Rd\|$	Rd	$\|Rd\|$	Rd	$\|Rd\|$	Rd	$\|Rd\|$
1	-	-	1.8	13.6	-5.0	8.7	-1.6	11.1
2	-	-	1.4	12.9	-0.8	10.4	0.3	11.7
3	-	-	-	-	-	-	-	-
4	-	-	2.2	23.5	-16.7	16.7	-7.3	20.1
5	1.3	11.1	-4.0	18.9	1.1	13.3	-0.1	13.6
6	-2.1	12.7	-6.8	13.0	6.8	18.1	-1.1	14.1
7	-5.0	12.7	-13.4	27.5	16.2	44.1	-1.8	24.2
8	-3.1	12.8	0.7	13.7	-1.3	13.6	-1.7	13.2
9	8.6	13.0	-9.8	14.7	-14.9	14.9	-1.9	13.9
10	2.9	11.4	3.7	15.8	-10.3	11.3	-0.2	12.5
11	3.1	12.1	1.4	31.8	-16.3	16.3	-2.2	18.1
12	5.5	12.6	3.0	18.4	-6.3	15.9	1.9	14.9
13	6.9	12.5	3.5	23.1	-10.7	10.7	1.6	14.7
14	2.9	12.2	4.5	19.9	-8.5	13.6	0.4	14.5
15	7.8	15.1	-6.8	6.8	-1.8	1.8	1.8	9.7
16	3.3	11.8	-3.2	17.6	-6.8	6.8	-0.9	12.0
17	3.9	11.7	-4.3	4.3	1.7	1.7	1.3	7.4
18	3.2	11.9	-11.7	11.7	-0.9	13.2	-1.5	12.2
19	10.0	14.0	-4.1	4.1	-0.9	0.9	3.7	8.3
20	-9.5	15.2	-2.6	21.4	2.3	9.3	-4.8	15.3
21	6.6	13.7	-2.0	2.0	6.6	6.6	4.5	9.0
22	-1.9	11.7	-2.3	2.3	5.6	5.6	-0.1	7.8
23	5.5	12.2	5.5	5.5	-0.3	0.3	4.0	7.5
24	6.9	12.9	-3.1	3.1	-1.9	1.9	2.2	7.7
25	-0.1	12.9	0.4	0.4	-4.6	4.6	-1.1	7.7
26	-1.9	12.5	4.4	14.3	-7.6	8.7	-1.8	12.0
27	10.1	34.0	-8.5	8.5	-20.1	20.1	-2.1	24.2
28	-2.7	13.4	3.6	9.8	-4.4	14.5	-1.6	12.8
Average	2.6	13.6	-1.7	13.3	-3.7	11.2	-0.4	13.0

REPORT DOCUMENTATION PAGE

Form Approved
OMB No. 0704–0188

1. REPORT DATE *(DD-MM-YYYY)*	2. REPORT TYPE	3. DATES COVERED *(From - To)*
01-03-2015	Technical Publication	

4. TITLE AND SUBTITLE
Badhwar - O'Neill 2014 Galactic Cosmic Ray Flux Model Description

5a. CONTRACT NUMBER

5b. GRANT NUMBER

5c. PROGRAM ELEMENT NUMBER

6. AUTHOR(S)
P. M . O'Neill and S. Golge and T. C. Slaba

5d. PROJECT NUMBER

5e. TASK NUMBER

5f. WORK UNIT NUMBER

7. PERFORMING ORGANIZATION NAME(S) AND ADDRESS(ES)
NASA Johnson Space Center
Houston, Texas 77058

8. PERFORMING ORGANIZATION REPORT NUMBER
S-1184

9. SPONSORING/MONITORING AGENCY NAME(S) AND ADDRESS(ES)
National Aeronautics and Space Administration
Washington, DC 20546-0001

10. SPONSOR/MONITOR'S ACRONYM(S)
NASA

11. SPONSOR/MONITOR'S REPORT NUMBER(S)
NASA/TP–2015–218569

12. DISTRIBUTION/AVAILABILITY STATEMENT
Unclassified-Unlimited
Subject Category 93
Availability: NASA STI Program (757) 864-9658

13. SUPPLEMENTARY NOTES
An electronic version can be found at http://ntrs.nasa.gov.

14. ABSTRACT
The Badhwar-O'Neill (BON) Galactic Cosmic Ray (GCR) model is based on GCR measurements from particle detectors. The model has mainly been used by NASA to certify microelectronic systems and the analysis of radiation health risks to astronauts in space missions. The BON14 model numerically solves the Fokker-Planck differential equation to account for particle transport in the heliosphere due to diffusion, convection, and adiabatic deceleration under the assumption of a spherically symmetric heliosphere. The model also incorporates an empirical time delay function to account for the lag of the solar activity to reach the boundary of the heliosphere. This technical paper describes the most recent improvements in parameter fits to the BON model (BON14). Using a comprehensive measurement database, it is shown that BON14 is significantly improved over the previous version, BON11.

15. SUBJECT TERMS
galactic cosmic radiation, GCR, Badhwar - O'Neill model

16. SECURITY CLASSIFICATION OF:			17. LIMITATION OF ABSTRACT	18. NUMBER OF PAGES	19a. NAME OF RESPONSIBLE PERSON
a. REPORT	b. ABSTRACT	c. THIS PAGE			STI Information Desk (email: help@sti.nasa.gov)
U	U	U	UU	32	19b. TELEPHONE NUMBER *(Include area code)* (757) 864-9658